NANO LETTERS
Letter
Cite This: Nano Lett. XXXX, XXX, XXX−XXX
pubs.acs.org/NanoLett

Static Modulation Wave of Arrays of Halogen Interactions Transduced to a Hierarchy of Nanoscale Change Stimuli of Crystalline Rotors Dynamics

Sergey Simonov,[†,‡] Leokadiya Zorina,[†,‡] Pawel Wzietek,[*,§] Antonio Rodríguez-Fortea,[∥] Enric Canadell,[*,⊥] Cécile Mézière,[†] Guillaume Bastien,[†] Cyprien Lemouchi,[†] Miguel A. Garcia-Garibay,[*,#] and Patrick Batail[*,†]

[†]Laboratoire MOLTECH-Anjou, CNRS UMR 6200, Université d'Angers, 49045 Angers, France
[‡]Institute of Solid State Physics, Russian Academy of Sciences, Chernogolovka, Moscow District 142432 Russia
[§]Laboratoire de Physique des Solides, CNRS UMR 6502, Université de Paris-Sud, 91405 Orsay, France
[∥]Departament de Química Física i Inorgànica, Universitat Rovira i Virgili, Marcel.li Domingo 1, 43007 Tarragona, Spain
[⊥]Institut de Ciència de Materials de Barcelona (ICMAB-CSIC), Campus de la UAB, 08193 Bellaterra, Spain
[#]Department of Chemistry and Biochemistry, University of California, Los Angeles, Los Angeles, California 90095, United States

Supporting Information

ABSTRACT: Here we present a study where what can be seen as a static modulation wave encompassing four successive arrays of interacting iodine atoms in crystalline 1,4-Bis((4′-(iodoethynyl)phenyl) ethynyl)bicyclo[2,2,2]octane rotors changes the structure from one-half molecule to three-and-a-half molecules in the asymmetric unit below a phase transition at 105 K. The remarkable finding is that the total ^{1}H spin−lattice relaxation rate, T_1^{-1}, of unprecedented complexity to date in molecular rotors, is the weighted sum of the relaxation rates of the four contributing rotors relaxation rates, each with distinguishable exchange frequencies reflecting Arrhenius parameters with different activation barriers (E_a) and attempt frequencies (τ_o^{-1}). This allows us to show in tandem with rotor-environment interaction energy calculations how the dynamics of molecular rotors are able to decode structural information from their surroundings with remarkable nanoscale precision.

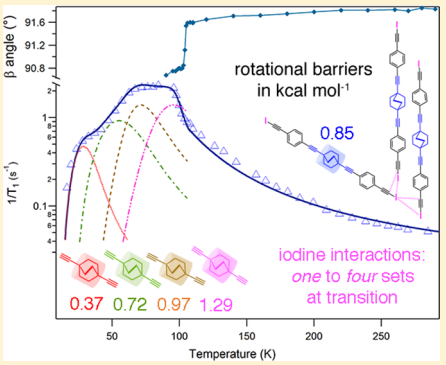

KEYWORDS: *Molecular rotors, self-assembly, solid state NMR, mechanism of rotation, DFT calculations, rotational barriers*

The growth or turning movement of an organism, usually a plant, illustrates how highly organized structures tend to respond in a complex but reliable manner when subject to environmental stimuli.[1,2] Understanding such events is important in the realms of materials chemistry and physics of molecular machines because the development of elaborate sensory devices with increasing levels of complexity is also required to accurately report changes that occur in the environment of their dynamic components.[3−20]

Here we present a study where the structure of the crystalline 1,4-bis((4′-(iodoethynyl)phenyl)ethynyl) bicyclo[2.2.2]octane rotor, **1** (Figure 1) changes at 105 K from one-half molecule to three-and-a-half molecules in the asymmetric unit. Below this phase transition, a periodic waving pattern, akin to an acoustic wave anchored in the lattice, encompasses in one period four successive self-assembled arrays[8−11] of interacting iodine atoms.[21−26] The remarkable finding is that the complex, total ^{1}H spin−lattice relaxation rate, T_1^{-1}, revealed by variable-temperature, variable-field experiments, is the weighted sum of the relaxation rates of the four contributing rotors relaxation rates. Hence, magnetic relaxation transforms from a process

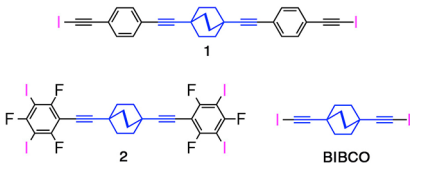

Figure 1. Structure of molecular rotor **1**. Together with **2**[9] and BIBCO[8,9] they are a class of crystalline rotors that self-assemble by iodine−iodine interactions. Both **2** and BIBCO were previously shown to display ambient temperature dynamics in the gigahertz regime. Preparation and characterization of compound **1** are described in the Supporting Information.

determined by a single molecular rotator in the high temperature phase into one that has distinguishable weighted contribution from the four new sites, each with distinguishable exchange frequencies reflecting Arrhenius parameters with

Received: March 14, 2018
Revised: May 2, 2018
Published: May 8, 2018

DOI: 10.1021/acs.nanolett.8b00956
Nano Lett. XXXX, XXX, XXX−XXX

different activation barriers (E_a) and attempt frequencies (τ_o^{-1}). This allows us to show in tandem with rotor-environment interaction energy calculations how the dynamics of molecular rotors are able to decode structural information from their surroundings with remarkable nanoscale precision.

Three intermolecular interactions involving iodine serve to direct the self-assembly of two-dimensional arrays of **1** (Figure 2). While δ_1 and δ_2 are common to **1** and 1,4-bis(iodoethynyl)-

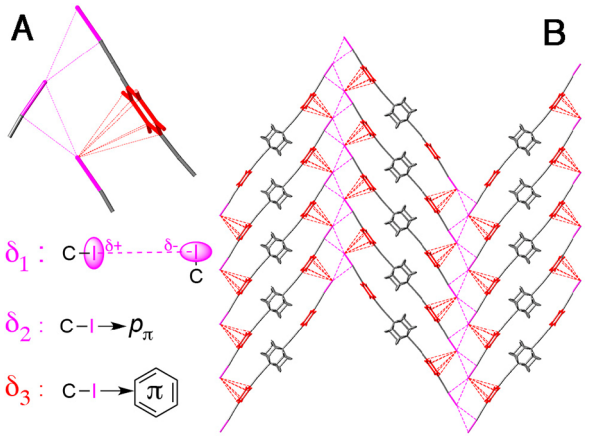

Figure 2. (A) The three types of intermolecular interactions involving iodine atoms and their schematic representations. (B) A single two-dimensional array self-assembled out of δ_1, δ_2, and δ_3 in the structure of **1** at 120 K. Note that only one out of the two equilibrium rotator positions are depicted here.

bicyclo[2.2.2]octane (BIBCO) (Figure S1), we show here that the installation of ethynylphenyl fragments on the BIBCO frame provides additional molecular degrees of freedom that expressed through C–I···π interaction δ_3,[27] confers a unique collective behavior to the dynamics of **1**.

We have observed that the monoclinic unit cell of a single crystal of **1** abruptly changes, experiencing below 105 K (Figure 3B) an expansion by seven times its volume to encompass three and a half independent rotators at 90 K, labeled I to IV in Figure 3C (only one-half independent rotor in the asymmetric unit is present in the structure of **1** at 120 K; details of the investigation of the reversible transition and structure refinements at 120 K, Figure 3A, and 90 K, Figure 3C, can be found in the Supporting Information and Figures S6–S10). It is even more remarkable that the layer-by-layer packing has each of the four homogeneous arrays of independent rotators stacked in alternating sequences, color-coded red (I), gold (II), blue (III), and black (IV) in Figure 3C. Moreover, the layers are stacked in registry yet alternately sliding by one-half molecular length. Thus, the interlayer interactions primarily involve C–H···I hydrogen interactions (Figure 3A,C) that define four distinct rotor-environment pockets. The origin of the differentiation of these pockets lies in what is seen as a static modulation wave of all three intermolecular interactions, δ_1, δ_2, and δ_3 (Figure 2), encompassing the four homogeneous layers of independent rotators I, II, III, and IV, typically adjusting the degree of freedom of the δ_3-interactions manifold. For example, note that all phenyl rings are parallel at 120 K; then see in Figure S10 the distribution of dihedral angles between two phenyl rings at 90 K, from 0° in IV, to 25.6°, 14.7° and 3.1° in I, II and III, respectively. Moreover, the single C–I···I–C interaction, δ_1 (I···I, 4.049 Å) at 120 K bursts at the transition into seven different interactions whose I···I distances (3.885 to 4.334 Å)

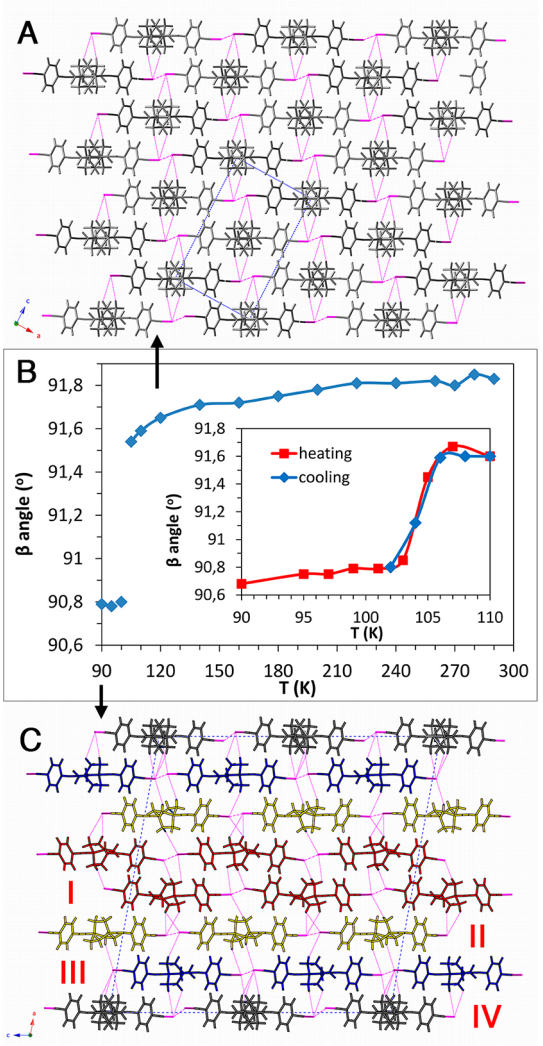

Figure 3. (A) Layer-by-layer packing of arrays of the single one-half independent rotators (disordered with balanced occupancies on two equilibrium positions) in the structure of **1** at 120 K. Dotted red lines are δ_1 interactions and C–H···I interactions by which the rotators rub on their environment. (B) The reversible structure transition (see also Figures S6–S9) illustrated by an abrupt change of the monoclinic angle β. (C) Below the transition, a static modulation wave of the three halogen interactions encompasses a registry of four different arrays (I–IV) shown here at 90 K. Note that only one rotator (IV) is disordered with balanced occupancies while all three other independent rotators have one equilibrium position only.

may be seen more as halogen contacts[26] yet are similar to those that direct the self-assembly and phase diagrams, both mediated by iodine···iodine interactions in **2**[9] and BIBCO.[8]

Variable-field ^{1}H and ^{13}C solid state NMR experiments carried out on static crystalline samples over large temperature and pressure windows have illuminated our understanding of the balance of competing electronic instabilities coupled to molecular degrees of freedom at the heart of the rich quantum physics in low dimension in strongly correlated molecular conductors.[28−32] Translating to the realm of molecular rotors the ability to perform variable-field, variable-temperature proton spin–lattice relaxation time experiments, ^{1}H T_1^{-1}, has recently demonstrated great promise to gain insight into the dynamics of crystalline rotors and, when appropriate, help disentangle multiple relaxation processes occurring all at once

DOI: 10.1021/acs.nanolett.8b00956
Nano Lett. XXXX, XXX, XXX−XXX

at the same spin temperature (see the basic principles in the Supporting Information).[12−17] Here, variable-temperature (20−300 K) proton spin−lattice relaxation experiments carried out at two ^{1}H Larmor frequencies on a polycrystalline sample of **1** reveal at the temperature of the structural transition a reversible discontinuity (Figure 4) similar to that occurring in

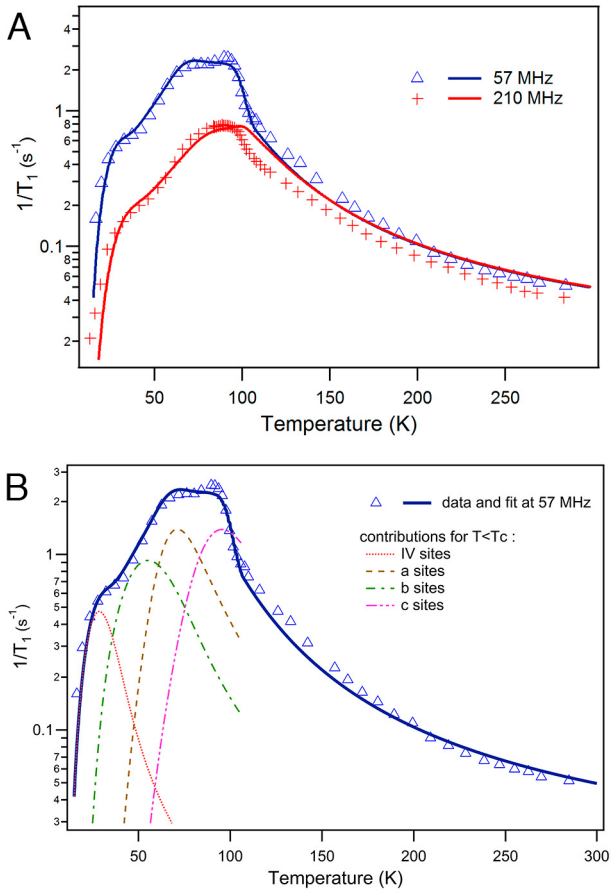

Figure 4. (A) Variable-temperature ^{1}H spin−lattice relaxation time T_1^{-1} at 57 and 210 MHz for **1**. The blue and red lines represent the fits[33,34] of the data to a sum of standard Kubo−Tomita expressions with thermally activated correlation times $\tau_i = \tau_0 \exp(E_i/kT)$ where E_i denotes the energy barrier at site i (see text and Supporting Information). (B) Curves for each of the four components of the total relaxation ($T < T_c$) drawn for one frequency.

2,[9] another extended analog of BIBCO also endowed with the additional degree of freedom conferred by two phenyl rings implemented in the rod axle (Figure 1).

Below the phase transition, the T_1^{-1} data display several entangled maxima. This is not unexpected since the analysis of the structure at 90 K led us to identify a total of four independent rotator sites that would result in complex dynamics encompassing as many independent relaxation processes. The intensity of T_1^{-1} maxima scales with the net number of moving ^{1}H on each independent site. Hence, the fits of the data to the Kubo−Tomita (KT) formula for T_1 with correlation times $\tau_i = \tau_0 \exp(E_i/kT)$ were conducted with the knowledge that below the transition rotators I, II, and III each involve two-sevenths of the total number of moving protons, and rotator IV having one-seventh of the net number. Therefore, the low-temperature data can be fitted with a weighted sum of four KT expressions with different energy barriers (Figure 4B and Supporting Information), hereafter noted E_a, E_b, E_c, E_{IV}. Note that the first three barriers refer to rotators I, II, and III and cannot be assigned solely from the fits because they have the same weight. On the other hand, all moving protons are located on a single independent site at 120 K. Therefore, above the transition temperature, T_c, the fit was done assuming a single barrier, noted E_{HT}. To simplify the fits, all processes were assigned a common attempt frequency (τ_o^{-1}). This is expected for identical rotors because τ_0 is a frequency characteristic of a specific, freely moving rotor. The best fit shown in Figure 4A was obtained with $\tau_0 = 1.8 \times 10^{-12}$ s.

For $T > T_c$, the fit yields $E_{HT} = 429$ K (0.85 kcal mol^{-1}). For the low-temperature phase, we could not obtain good fits with fixed barriers, which led us to assume the existence of a slight disorder implying a distribution of energy barriers. A Gaussian distribution was then set for each barrier with the σ-values of their respective relative widths given below in percent of the barrier values (Table S2). Likewise, we assumed a slight distribution of the transition temperature T_c in the fit. The fits shown in Figure 4 yield $E_{IV} = 188$ K (0.37 kcal mol^{-1}) and $\sigma_{IV} = 20\%$; three additional energy barriers are $E_a = 360$ K (0.72 kcal mol^{-1}), $\sigma_a = 22\%$; $E_b = 486$ K (0.97 kcal mol^{-1}), $\sigma_b = 1.2\%$; $E_c = 651$ K (1.29 kcal mol^{-1}), $\sigma_c = 1.9\%$; $T_c = 100$ K, $\sigma_{T_c} = 3.6\%$ (Table S3) to be assigned to the motion of rotators in sites within layers I, II ,and III.

Assigning relaxation processes at the nano- and microscale, be they discrete events on distinct sites[8,9,12−14] or dual, coupled processes associated with correlated rotational motion in well-separated pairs of rotators,[13,15−17] requires the fits to the T_1^{-1} data to be coupled to calculations[9,12−17] of rotor-environment interaction energies (Table S3). Thus, we have estimated the five rotational barriers (Figure 5) for each independent rotator

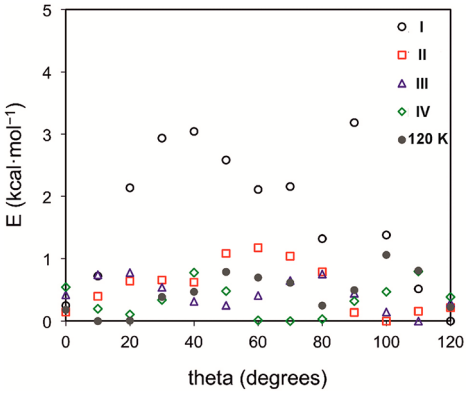

Figure 5. Computed energy profiles (in kcal mol^{-1}) for the rotation of each independent rotator surrounded by their neighbor molecules; the five models for the DFT transition structures are described in Figure S11.

by means of partial geometry optimizations (rotor itself and the nearest molecules of the environment interacting with it through iodine atoms) using the same computational details reported previously.[12]

All barriers (Figure 5 and Figure S11) are calculated around 1 kcal mol^{-1} (0.78−1.18) except that for rotator I in the 90 K structure which is noticeably higher at 3.19 kcal mol^{-1} (1605 K). This is because shorter H···I contacts occur in the transition state for I, including a contact as short as 2.94 Å. In contrast, rotators in sites II, III, and IV have no contact shorter than 3.2

DOI: 10.1021/acs.nanolett.8b00956
Nano Lett. XXXX, XXX, XXX−XXX

Å when the geometry of their transition structures is optimized along their rotational trajectories. For example, the shorter H···I contact for II, the 120 K rotator, and IV are 3.20−3.21 Å; they are even larger, that is, 3.28 Å for III. Therefore, the activation barriers seem to be primarily determined by the strength of the shorter H···I contact in their transition state.

Moreover, the values of the calculated barriers in Figure 5 allow for the assignment (Table S2 and Figure S11) of the rotational barriers extracted from the fits of the T_1^{-1} data between 20 and 300 K. Both are fully coherent and qualify a global rotor dynamics characterized by one large rotational barrier supplemented by two pairs of smaller ones separated by ∼124 K (proton spin−lattice experiments) or ∼166 K (rotor-environment energy calculations). The remarkable agreement demonstrated here testifies the validity of this integrated approach.

Beyond the nanoscale change stimuli of the present crystalline rotor dynamics, providing information on their surroundings with a remarkable level of accuracy, other concerted changes are hidden in rich phase diagrams to be disclosed by opening large temperature windows, integrating structure, spin−lattice relaxation, dielectric and second-order nonlinear optical experiments, and rotor-environment energy calculations. Unraveling the phase diagrams of these materials, also tackling in future work their response to uniaxial and isostatic pressure, is interesting because they could be used as simulators to control molecular machines.

In addition to drawing attention to the susceptibility of extended, noncovalent arrays of interacting halogen atoms to undergo concerted modulation in their temperature phase diagrams,[8,9] the results observed with compound **1** provide[8,9,12−17] the kind of in-depth insight on the mechanism of motion required on the way toward a control of molecular machines at the nanoscale.[3−7]

■ ASSOCIATED CONTENT

Supporting Information

The Supporting Information is available free of charge on the ACS Publications website at DOI: 10.1021/acs.nanolett.8b00956.

Supporting figures and tables; synthesis; VT ^{1}H spin−lattice relaxation time: basic principles and experimental details, computational details (PDF)

Crystal structures at 120 K (CIF)

Crystal structures at 90 K (CIF)

■ AUTHOR INFORMATION

Corresponding Authors

*E-mail: pawel.wzietek@u-psud.fr.
*E-mail: canadell@icmab.es.
*E-mail: mgg@chem.ucla.edu.
*E-mail: patrick.batail@univ-angers.fr.

ORCID

Antonio Rodríguez-Fortea: 0000-0001-5884-5629
Enric Canadell: 0000-0002-4663-5226
Miguel A. Garcia-Garibay: 0000-0002-6268-1943
Patrick Batail: 0000-0001-7125-5009

Notes

The authors declare no competing financial interest.

CCDC 1577087 and 1577088 contain the crystallographic data for this paper. These data can be obtained free of charge from The Cambridge Crystallographic Data Centre.

■ ACKNOWLEDGMENTS

This research was funded by the CNRS, the University of Angers, the University of Paris-Sud, Orsay; the Région des Pays de la Loire Grant MOVAMOL, the joint CNRS-Russian Federation grants PICS 6028 and RFBR-CNRS 12-03-91059 (Chernogolovka). Work at UCLA was supported by U.S.A. National Science Foundation Grants DMR140268 and DMR-1700471. Work in Bellaterra and Tarragona was supported by the Spanish Ministerio de Economía y Competitividad (Grants FIS2015-64886-C5-4-P and CTQ2017-87269-P) and Generalitat de Catalunya (2017SGR1506 and 2017SGR629). E.C. acknowledges support by MINECO (Spain) through the Severo Ochoa Centers of Excellence Program (Grant SEV-2015-0496). S.S. thanks the CNRS for a postdoctoral grant and C.L. and G.B. thank the Région des Pays de la Loire for Ph.D. grants, respectively. L.Z. thanks the CNRS for an Associated Researcher Fellowship.

■ REFERENCES

(1) Kocsis, L. S.; Elbel, K. M.; Hardigree, M. A.; Brummond, K. M.; Haidekker, M. A.; Theodorakis, E. A. *Org. Biomol. Chem.* **2015**, *13*, 2965.
(2) Pickard, B. G. *Curr. Top. Membr.* **2007**, *58*, 361.
(3) Abendroth, J. A.; Bushuyev, O. S.; Weiss, P. S.; Barrett, C. J. *ACS Nano* **2015**, *9*, 7746.
(4) Erbas-Cakmak, S.; Leigh, D. A.; McTernan, C. T.; Nussbaumer, A. L. *Chem. Rev.* **2015**, *115*, 10081.
(5) Domingos, S. R.; Cnossen, A.; Buma, W. J.; Browne, W. R.; Feringa, B. L.; Schnell, M. *Angew. Chem., Int. Ed.* **2017**, *56*, 11209.
(6) Nishiyama, H.; Takeda, T.; Hoshino, N.; Takahashi, K.; Noro, S.-I.; Nakamura, T.; Akutagawa, T. *Cryst. Growth Des.* **2018**, *18*, 286.
(7) Vogelsberg, C. S.; Garcia-Garibay, M. A. *Chem. Soc. Rev.* **2012**, *41*, 1892.
(8) Lemouchi, C.; Vogelsberg, C.; Simonov, S.; Zorina, L.; Batail, P.; Brown, S.; Garcia-Garibay, M. *J. Am. Chem. Soc.* **2011**, *133*, 6371.
(9) Lemouchi, C.; Yamamoto, H. M.; Kato, R.; Simonov, S.; Zorina, L.; Rodríguez-Fortea, A.; Canadell, E.; Wzietek, P.; Iliopoulos, I.; Gindre, D.; Chrysos, M.; Batail, P. *Cryst. Growth Des.* **2014**, *14*, 3375.
(10) Catalano, L.; Peŕez-Estrada, S.; Terraneo, G.; Pilati, T.; Resnati, G.; Metrangolo, P.; Garcia-Garibay, M. A. *J. Am. Chem. Soc.* **2015**, *137*, 15386.
(11) Catalano, L.; Perez-Estrada, S.; Wang, H.-H.; Ayitou, A. J.-L.; Khan, S. I.; Terraneo, G.; Metrangolo, P.; Brown, S.; Garcia-Garibay, M. A. *J. Am. Chem. Soc.* **2017**, *139*, 843.
(12) Lemouchi, C.; Mézière, C.; Zorina, L.; Simonov, S.; Rodríguez-Fortea, A.; Canadell, E.; Wzietek, P.; Auban-Senzier, P.; Pasquier, C.; Giamarchi, T.; Garcia-Garibay, M. A.; Batail, P. *J. Am. Chem. Soc.* **2012**, *134*, 7880.
(13) Lemouchi, C.; Iliopoulos, K.; Zorina, L.; Simonov, S.; Wzietek, P.; Cauchy, T.; Rodríguez-Fortea, A.; Canadell, E.; Kaleta, J.; Michl, J.; Gindre, D.; Chrysos, M.; Batail, P. *J. Am. Chem. Soc.* **2013**, *135*, 9366.
(14) Bastien, G.; Lemouchi, C.; Wzietek, P.; Simonov, S.; Zorina, L.; Rodríguez-Fortea, A.; Canadell, E.; Batail, P. *Z. Anorg. Allg. Chem.* **2014**, *640*, 1127−1133.
(15) Bastien, G.; Lemouchi, C.; Allain, M.; Wzietek, P.; Rodríguez-Fortea, A.; Canadell, E.; Iliopoulos, K.; Gindre, D.; Chrysos, M.; Batail, P. *CrystEngComm* **2014**, *16*, 1241.
(16) Kaleta, J.; Michl, J.; Mézière, C.; Simonov, S.; Zorina, L.; Wzietek, P.; Rodríguez-Fortea, A.; Canadell, E.; Batail, P. *CrystEngComm* **2015**, *17*, 7829.

DOI: 10.1021/acs.nanolett.8b00956
Nano Lett. XXXX, XXX, XXX−XXX

(17) Rodriguez-Fortea, A.; Kaleta, J.; Mézière, C.; Allain, M.; Canadell, E.; Wzietek, P.; Michl, J.; Batail, P. *ACS Omega* **2018**, *3*, 1293−1297.
(18) Comotti, A.; Bracco, S.; Sozzani, P. *Acc. Chem. Res.* **2016**, *49*, 1701.
(19) Comotti, A.; Bracco, S.; Yamamoto, A.; Beretta, M.; Hirukawa, T.; Tohnai, N.; Miyata, M.; Sozzani, P. *J. Am. Chem. Soc.* **2014**, *136*, 618.
(20) Bracco, S.; Castiglioni, F.; Comotti, A.; Galli, S.; Negroni, M.; Maspero, A.; Sozzani, P. *Chem. - Eur. J.* **2017**, *23*, 11210.
(21) Legon, A. C. *Phys. Chem. Chem. Phys.* **2010**, *12*, 7736.
(22) Fourmigué, M. *Curr. Opin. Solid State Mater. Sci.* **2009**, *13*, 36.
(23) Bertani, R.; Sgarbossa, P.; Venzo, A.; Lelj, F.; Amati, M.; Resnati, G.; Pilati, T.; Metrangolo, P.; Terraneo, G. *Coord. Chem. Rev.* **2010**, *254*, 677.
(24) Troff, R. W.; Mäkelä, T.; Topic, F.; Valkonen, A.; Raatikainen, K.; Rissanen, K. *Eur. J. Org. Chem.* **2013**, *2013*, 1617.
(25) Meyer, F.; Dubois, P. *CrystEngComm* **2013**, *15*, 3058.
(26) Desiraju, G. R.; Ho, P. S.; Kloo, L.; Legon, A. C.; Marquardt, R.; Metrangolo, P.; Politzer, P.; Resnati, G.; Rissanen, K. *Pure Appl. Chem.* **2013**, *85*, 1711.
(27) Cao, J.; Yan, X.; He, W.; Li, X.; Mo, Y.; Liu, M.; Jiang, T.-B.; et al. *J. Am. Chem. Soc.* **2017**, *139*, 6605.
(28) Zorina, L.; Simonov, S.; Mézière, C.; Canadell, E.; Suh, S.; Brown, S. E.; Foury-Leylekian, P.; Fertey, P.; Pouget, J.-P.; Batail, P. *J. Mater. Chem.* **2009**, *19*, 6980−6994.
(29) Baudron, S. A.; Batail, P.; Coulon, C.; Clérac, R.; Canadell, E.; Laukhin, V.; Melzi, R.; Wzietek, P.; Jérome, D.; Auban-Senzier, P.; Ravy, S. *J. Am. Chem. Soc.* **2005**, *127*, 11785−11797.
(30) Miyagawa, K.; Kanoda, K.; Kawamoto, A. *Chem. Rev.* **2004**, *104*, 5635−5653.
(31) Lefebvre, S.; Wzietek, P.; Brown, S.; Bourbonnais, C.; Jérome, D.; Mézière, C.; Fourmigué, M.; Batail, P. *Phys. Rev. Lett.* **2000**, *85*, 5420−5423.
(32) Mayaffre, H.; Wzietek, P.; Lenoir, C.; Jérome, D.; Batail, P. *Europhys. Lett.* **1994**, *28*, 205−210.
(33) Multi-parameter fits of the NMR relaxation were done using a genetic optimization algorithm; see for example Wormington, M.; Panaccione, C.; Matney, K. M.; Bowen, D. K. *Philos. Trans. R. Soc., A* **1999**, *357*, 2827−2848.
(34) Nelson, A. *J. Appl. Crystallogr.* **2006**, *39*, 273.

DOI: 10.1021/acs.nanolett.8b00956
Nano Lett. XXXX, XXX, XXX−XXX